Multipath Scintillation Statistics Obtained From RF Measurements Near the Earth's Surface

H. T. Yura and S. M. Beck

***Abstract*— We report on 1.78 GHz RF near-horizontal multipath propagation measurements, in both California and New Hampshire, taken over various links where there is no direct clear line of sight. This report deals specifically with the time-dependent fluctuations of the RF signal, which were observed in the time history of the received signals at various sites. We characterize and discuss the general statistical features of multipath scintillation and discuss the differences between the orders of magnitude enhanced scintillation index (SI) (defined as the variance of the received RF power divided by the square of the mean of the RF power) observed for multipath and that obtained for clear line-of-sight paths. To the best of our knowledge, for the first time reported in the literature, we have observed and statistically quantified multipath scintillation conditions where the SI is both of the order and greater than unity. The observed probability distributions of multipath scintillation are compared with several candidate distributions, and the Nakagami-m and the gamma–gamma distribution emerge as the preferred distributions for weak-to-moderate and moderate-to-strong scintillation conditions, respectively. The observed level crossing statistics of the multipath signal is compared with theory, where good agreement is obtained for all cases of concern.**

***Index Terms*— Atmospheric propagation, level crossing statistics, multipath, scintillation, turbulence.**

I. Introduction

THIS paper deals specifically with the time-dependent fluctuations of the RF signal observed in the time history of received signals along various propagation paths.

The majority of studies in the literature on RF scintillation near the ground deal with the fluctuations below the mean or signal fades. Few have been concerned with the potential for scintillation to produce RF power at a receiver significantly above the mean. These cases must be taken into account when looking at potential interference to other systems operating in the same frequency range. Most of the studies discussing RF scintillation for horizontal near-ground trajectories consider the direct lines of sight between the transmitter and receiver and thus experience simultaneous free-space and multipath effects. In our case, only one out of more than 19 cases involved a direct line of sight because terrain blocked the direct view between the transmitter and receiver at all of the other receiving locations. Also, the majority of the studies in the literature on RF scintillation near the ground deal with the fluctuations below the mean or fades, as they produce the potential for loss of information on communications links or signal for radar systems. Few have been concerned with the potential for scintillation to produce RF power at a receiver significantly above the mean. One of these, an ITU model [1], does include enhancements as well as fades but on a very gross geographic scale. This model averages behavior over areas more than 100 km square, whereas our studies show very large (10–30 dB) variability of the fluctuations on a spatial scale 10 times smaller. These fluctuations are important in the context of this study because they can produce significantly higher RF powers at a specific location than predicted by the propagation models, which only provide a mean value of power. In particular, we have identified those sites where enhancement levels of greater than 6 dB above the mean power level were observed. These observed RF power fluctuations are all caused by scintillation of the RF beam due to multipath effects modulated by the atmospheric index of refraction fluctuations. The general magnitude of the fluctuations can best be described by a term called the "scintillation index," or SI, which is the variance of the received RF power divided by the square of the mean of the RF power. We describe below the theoretical statistical treatment of these fluctuations and show by comparison with the measurements that their amplitude, duration, and likelihood of occurrence are quantitatively described by the theory. While the physical basis for the observed fluctuations is understood, and the theory can provide the statistical agreement for the above quantities from a given set of topographic and meteorological conditions and a measured SI, it is important to realize that it is not predictive for an arbitrary set of these conditions. The fluctuations are a result of the complicated superposition of fields associated with potentially many different multipaths, each having a phase affected differently by the local index of refraction fluctuations. Currently, not enough is known to be able to provide such quantitative *a priori* predictions, and additional work is required, which is beyond the scope of this effort.

Here, we report on measurements taken in California during March and July 2016 and in New Hampshire during April 2016. Finally, we note that the results presented here pertain primarily to rural/suburban environments and do not necessarily apply to urban environments.

The remainder of this paper is outlined as follows. In Section II, we review some relevant clear line-of-sight RF propagation theory through turbulence near the ground and obtain results for both the maximum expected SI as a function of propagation distance and provide the qualitative features of the corresponding power spectrum. In Section III-A,

Manuscript received August 28, 2017; revised July 2, 2018; accepted September 8, 2018. Date of publication October 22, 2018; date of current version January 16, 2019. *(Corresponding author: H. T. Yura.)*

The authors are with the Electronics and Photonics Laboratory, The Aerospace Corporation, Los Angeles, CA 90009 USA (e-mail: hal.t.yura@aero.org).

Color versions of one or more of the figures in this paper are available online at http://ieeexplore.ieee.org.

Digital Object Identifier 10.1109/TAP.2018.2877302

we review some of the observed signal characteristics that include some unaccounted for anomalous behavior. In Section III-B, we discuss the general observational features of multipath scintillation and discuss the differences between both the orders of magnitude enhanced observed multipath SI and that obtained for clear line-of-sight paths and the clear line-of-sight power spectrum. To the best of our knowledge, for the first time reported in the literature, we have observed and statistically quantified multipath scintillation conditions where the SI is both of the order and greater than unity. In Section III-C, the observed probability distributions of multipath scintillation are compared with several candidate distributions, and the Nakagami-m and the gamma–gamma distributions emerge as the preferred distributions for weak-to-moderate and moderate-to-strong scintillation conditions, respectively. In Section III-D, we discuss some relevant aspects of level crossing statistics. Specifically, the percentage of time the signal is above a threshold level above the mean, the corresponding crossing rate, and the mean duration of an enhanced level above the mean is of particular concern. The observed level crossing statistics of the multipath signal is compared with theory, where good agreement is obtained for all cases of concern. Finally, in Section IV, we discuss our results and provide some concluding remarks.

II. Scintillation: Direct Clear Line-of-Sight Propagation Paths

Briefly, the measurements were made by having the large transmit antenna align its azimuthal pointing angle to the exact bearing to the receive antenna. In all cases, the transmitter antenna elevation angle was required to comply with the so-called transmit inhibit zone, which varied as a function of azimuthal angle from about 0.7° to 2° above horizontal. Both the transmitter and receiver were similarly circularly polarized.

The station transmits a continuous tone, at typically 1 kW of RF power. The antenna's full-width at half-maximum main beamwidth is approximately 0.5°. The receive antenna is a relatively small 8 cm-diameter aperture antenna with a 3dB gain. The output of the antenna is fed to a spectrum analyzer (SA) for signal recording. For the time history measurements reported here, the SA is set to collect "zero span" with a frequency bandwidth of 100 Hz and a sampling frequency of 60 Hz. At this sample rate, 10 min of signal (i.e., 36 000 data points) can be recorded before the buffer needs to be read out. Ground-based weather stations at both the transmit and receive sides of the link collect local temperature, relative humidity, and wind data.

All receiving locations in this paper are well in the far field of the transmitter, and the receiving aperture diameter is sufficiently small so that aperture-averaging effects can be ignored. For a line-of-sight propagation path, fluctuations of received power are due to temporally random fluctuations of the index of refraction along the path [2]. The strength of the index of refraction irregularities along the propagation path is characterized by the so-called index structure constant $C_n^2(s)$, where "s" denotes the position along the path. At RF frequencies between about 1 MHz and 30 GHz, the index of refraction is independent of frequency, and the corresponding fluctuations are primarily due to fluctuations of humidity along the propagation path [3].

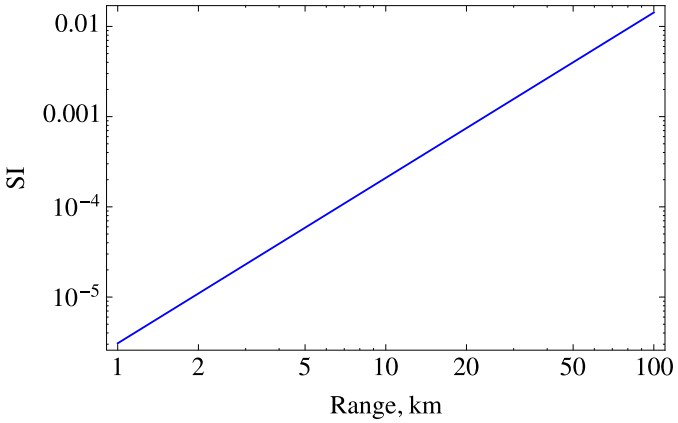

Fig. 1. Maximum expected clear line-of-sight SI at 1.78 GHz as a function of range.

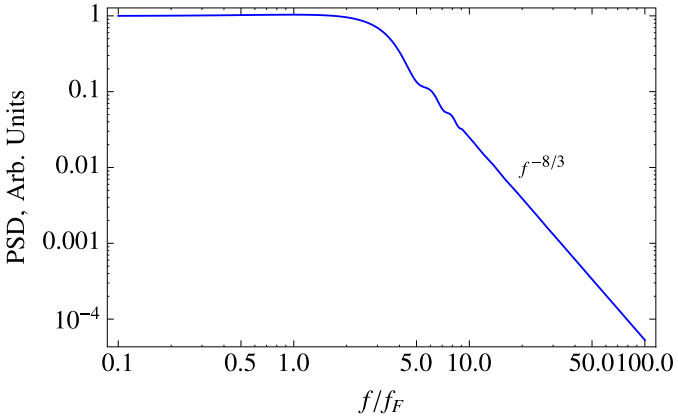

Fig. 2. Power spectra of direct line-of-sight scintillation for spherical waves as a function of normalized frequency, $f_N = f/f_F$, where f_F is the Fresnel frequency, and v is the wind speed normal to the line of sight. This curve ignores receiver aperture averaging and is based on the Kolmogorov model of tropospheric turbulence.

A central parameter in the characterization of the statistical distribution of received power is the SI defined as the variance of received power, P, normalized to the square of its mean value. We have

$$\mathrm{SI} = \frac{\langle \mathrm{P}^2 \rangle - \langle \mathrm{P} \rangle^2}{\langle \mathrm{P} \rangle^2} \tag{1}$$

where angular brackets denote the ensemble average.

For all cases of interest in this paper, the clear line of sight $\mathrm{SI} \ll 1$, and it is well established that in this case, the so-called weak scintillation regime, we have [4], [5]

$$\begin{aligned} \mathrm{SI} &= \exp\left[\sigma_{\ln I}^2\right] - 1 \\ &\cong \sigma_{\ln I}^2, \quad \text{for } \sigma_{\ln I}^2 \ll 1 \end{aligned} \tag{2}$$

where the log-intensity variance $\sigma_{\ln I}^2 \ll 1$. For the direct clear line-of-sight paths encountered here, the receiver is in the far field of the transmitter, and it can be shown that [1], [4]

$$\sigma_{\ln I}^2 = 2.25 k^{7/6} \int_0^L C_n^2(s)[s(1 - s/L)]^{5/6}\, ds \tag{3}$$

where L denotes the path length and k is the electromagnetic wavenumber (i.e., $k = 2\pi/\lambda$, where λ is the wavelength).

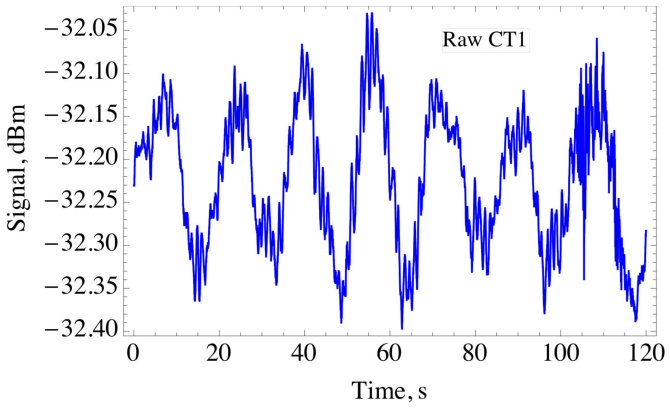

Fig. 3. Two-minute time segment of the received CT1 power.

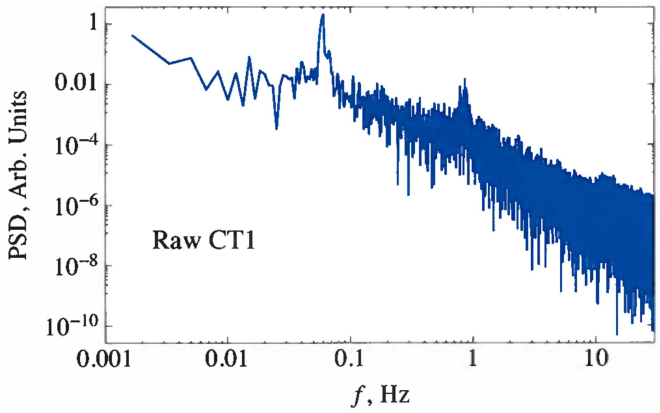

Fig. 4. Raw PSD of the CT1signal.

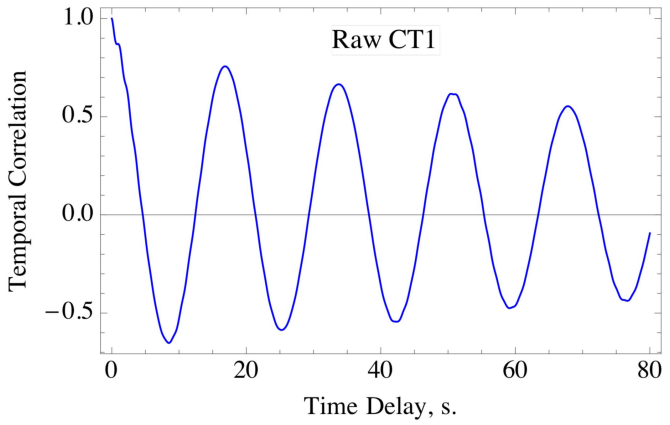

Fig. 5. Temporal correlation coefficient as a function of time delay of the (raw) CT1 data.

A rather comprehensive reference list of line-of-sight scintillation studies by other researchers is given at the end of [4, Ch. 3].

Microwave measurements of the vertical profile of C_n^2 were first measured directly by a single 9.4 GHz refractometer carried aloft on a light aircraft over Colorado and Florida [6]. Measurements were made from very close to the ground up to 29 000 ft. A large range of values was encountered in doing so

$$10^{-17}\ \mathrm{m}^{-2/3} < C_n^2 < 3 \times 10^{-13}\ \mathrm{m}^{-2/3}. \tag{4}$$

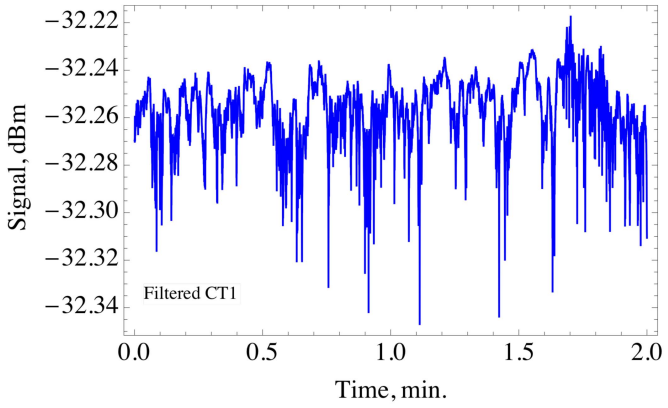

Fig. 6. Two-minute time segment of the filtered CT1 signal.

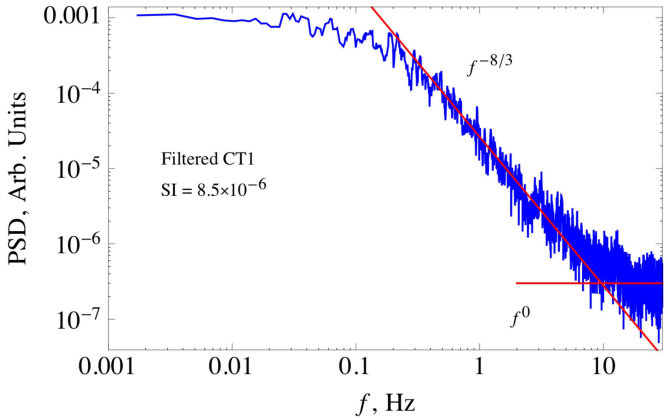

Fig. 7. Filtered PSD of the CT1signal.

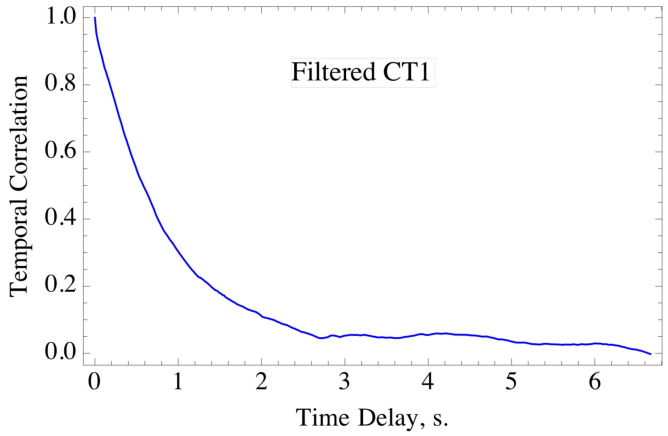

Fig. 8. Temporal correlation coefficient as a function of time delay of the filtered CT1 data.

As indicated in [3, Fig. 4], C_n^2 values of the order 10^{-13} $\mathrm{m}^{-2/3}$ were observed near the ground up to about 10 000 ft. These measurements are approximately 2 orders of magnitude greater than the optical values below 10 000 ft because of the strong contribution of water vapor to the microwave index of refraction irregularities. For reference purposes, Fig. 1 shows the plot as a function of range for $C_n^2 = 3 \times 10^{-13}$ $\mathrm{m}^{-2/3}$ of the maximum clear line-of-sight SI that would be expected at a microwave frequency of 1.78 GHz. For example, at the California Test Site-1 (CT1)

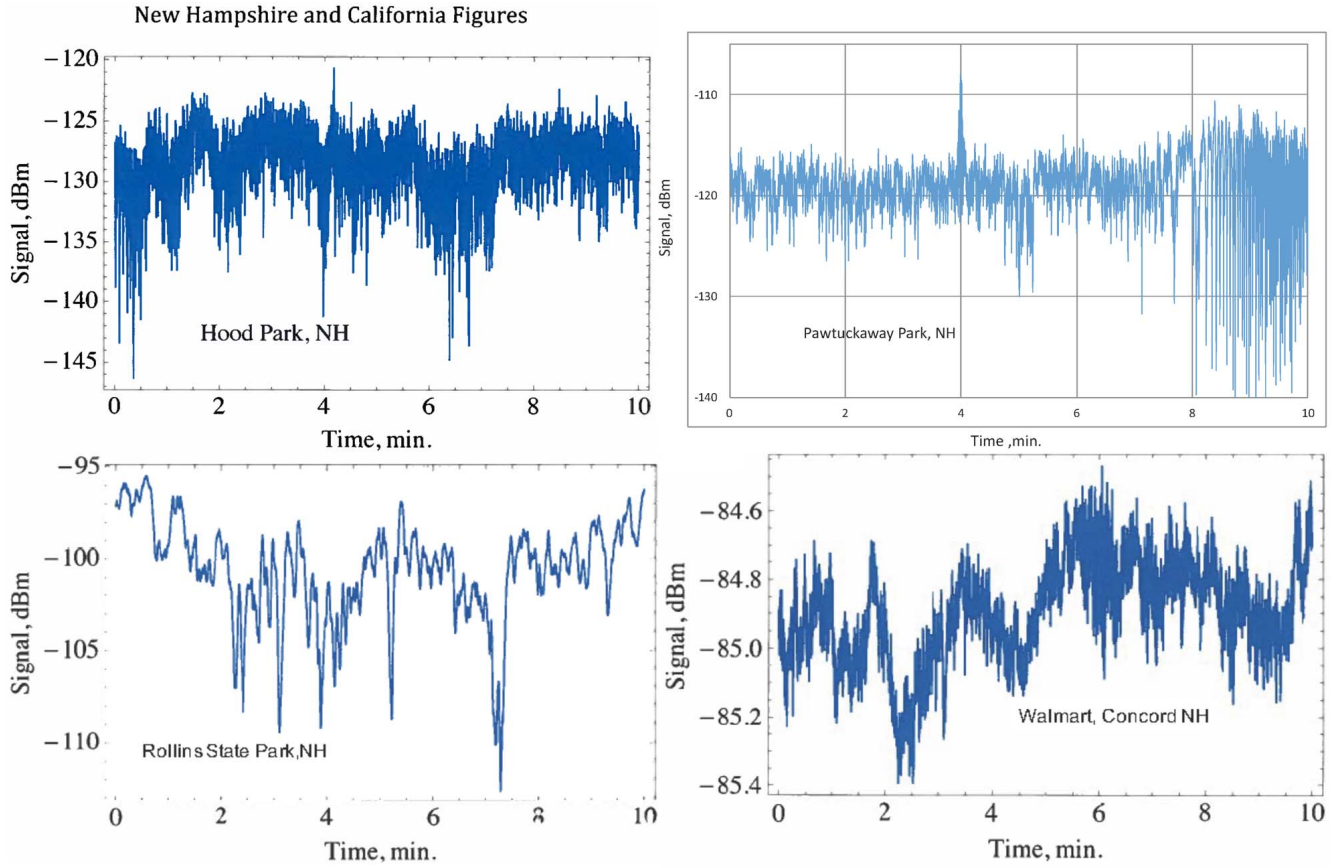

Fig. 9. Signal time series observed at Hood Park, Pawtuckaway Park, Rollins Park, and the Walmart, Concord New Hampshire sites.

site range of 6.1 km, we expect that an SI of no greater than about 8.4×10^{-5} to be obtained. Thus, for all propagation links, in both California and New Hampshire, negligible turbulence-induced power fluctuations are expected from clear line-of-sight propagation paths.

Furthermore, for line-of-sight propagation paths in the weak scintillation regime, it can be shown theoretically, and experimentally verified, as shown in Fig. 2, that the power spectral density (PSD) of the fluctuations is relatively flat at low frequencies f, while the high-frequency portion of the spectrum asymptotically falls off as $f^{-8/3}$ (see [4, Ch. 5]). In practice, we expect that the PSD exhibits a $f^{-8/3}$ high-frequency falloff until it hits the noise floor of the receiving system where it, then, tends to a constant representing uncorrelated white noise.

Of the numerous propagation measurements made, only one clear line-of-sight link in California was available at a site designated as CT1. Fig. 3 shows the two-minute time series segment of the raw CT1 site signal power. As shown in Fig. 4 of the corresponding PSD, the raw signal power data are compromised with cyclofrequency artifacts of about 0.06 and 0.83 Hz, respectively. The sources of these artifacts are unknown. This can be seen more clearly in Fig. 5 where the corresponding temporal correlation function of the raw CT1 site data is plotted as a function of time delay. Examination of Fig. 5 also reveals that in addition to a strong correlation at 16.67 s time delay, as indicated at very small time delays, there is a weaker correlation at about 0.8 s of time delay, which corresponds in frequency to about 0.06 and 0.83 Hz, respectively. We have filtered the raw CT1 site data using bandpass filters and removed the two cyclofrequency artifacts, and the resulting time series segment, PSD, and corresponding temporal correlation function are shown in Figs. 6–8, respectively. The SI of the filtered CT1 site signal is 8.5×10^{-6}, which is well representative of atmospheric turbulence-induced scintillation, in accordance with the results shown in Fig. 1, and the PSD is qualitatively in excellent agreement with that of the theoretical PSD shown in Fig. 2.

III. Scintillation: Nonline-of-Sight Multipath Propagation Paths

A. General Comments and Signal Characteristics

Because of terrain blockage between transmit antennas and various surrounding receiving sites in California (except the CT1 site) and New Hampshire, there are no clear line-of-sight propagation paths between the transmitter and the receiver. Terrain profiles of two representative propagation paths are shown in the Appendix along with their locations on a map and photographs of the receiver site surroundings. Thus, the received signal consists of a summation of an (unknown) multitude of independent indirect path contributions due to reflections from surrounding objects and inversion layers, ducting, and diffraction over the intervening terrain. For example, an important cause of multipath propagation is the existence of the layered structure in the troposphere where the refractive index no longer varies smoothly with height but

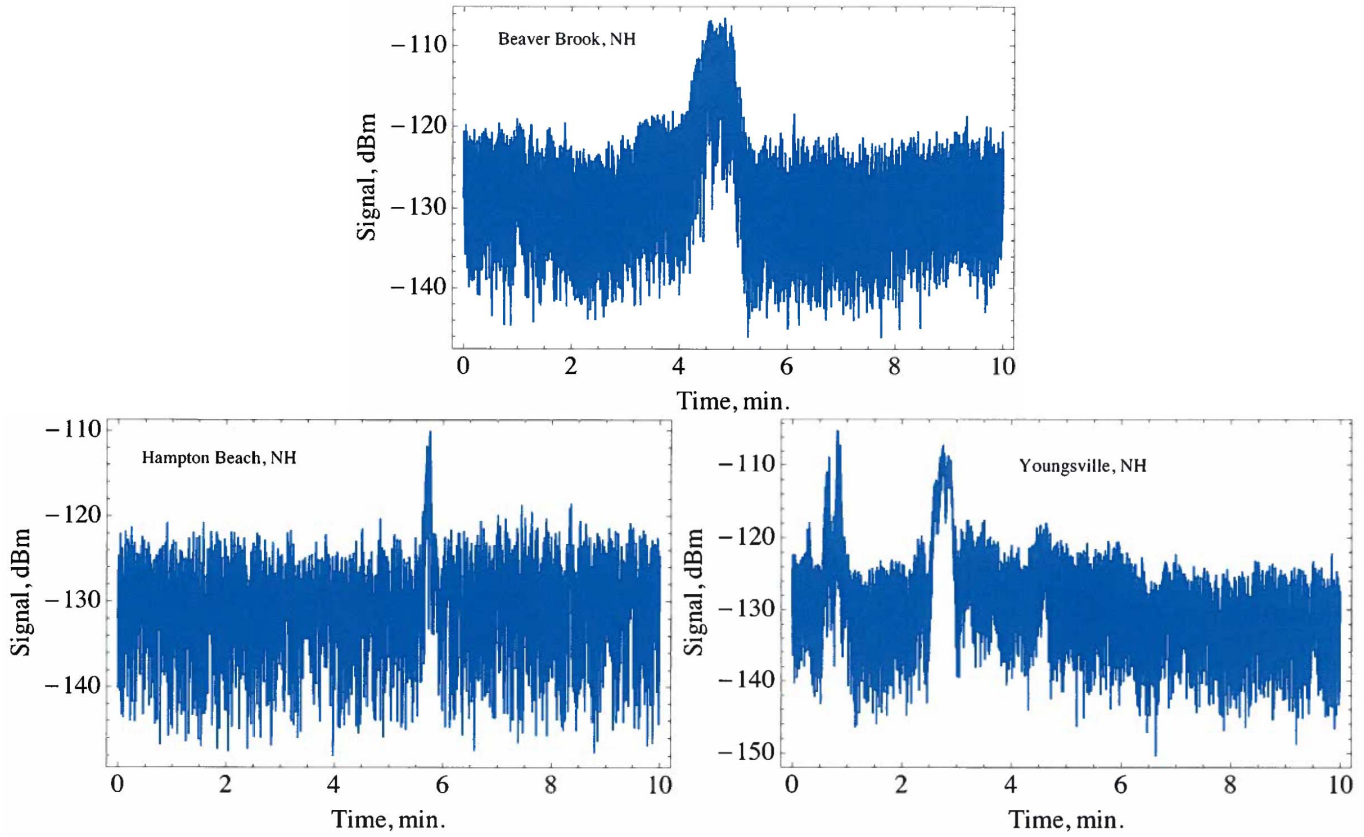

Fig. 10. Signal time series observed at the Beaver Brook, Hampton Beach, and Youngsville, New Hampshire sites.

has discontinuities where it changes rapidly. Lane *et al.* [7] have observed such layering, and a gradient of 1 N/m within layers of 10 m was detected. The results from the NOAA high resolution rapid refresh numerical weather models obtained for contemporaneous times to the measurements confirm the existence of ducting layers in several of the California locations.

In general, each of these independent contributions is temporally a random function of amplitudes, phases, and directions of arrival. The temporal fluctuations are due to reflection and scattering from moving objects such as wind-induced foliage motion and propagation through turbulent eddies along various propagation paths. In addition, various signal components can be Doppler shifted by different amounts due to the motion of intervening objects from which the RF energy reflects or scatters.

An exact solution for the multipath SI requires the knowledge and nature of the distribution and the correlations of all of the partial waves composing the total signal and becomes infeasible due to its inherent complexity, and no one has yet predicted this from the first principles. In addition, as indicated in the following, in many (but not all) of the multipath signal time series, the situation is complicated still further where there are indications of intermittency over relatively short time scales. This implies that C_n^2 and other turbulence parameters are changing continuously. The physics of these spontaneous events is not well understood. The basic concept is that turbulence itself gives rise to the bursts of energy at both large and small spatial scales. Random pulsations of both temperature and humidity are manifestations of intermittency and are an integral property of the turbulent flow field. This behavior is believed to be a natural consequence of hydrodynamics and is overlaid on the familiar process of subdivision of turbulent eddies but has not yet been derived from of the Navier–Stokes equation. Spontaneous columns of water vapor moving through multipath propagation paths manifest intermittency at microwave frequencies. In any event, the resulting multipath SI, as is indicated in the following, can be many orders of magnitude greater than the SI obtained for clear line-of-sight paths. This is primarily due to the relatively independent stochastic phase changes of the indirect path contributions that result in temporally mutually constructive and destructive interferences of the received signal. Due to the complexities alluded to above and to the best of our knowledge, no general theory and/or trends of multipath effects are available in the literature.

Several different signal characteristics were observed at various sites surrounding the transmitters. The most common features, as observed at Miller Park, Hood Park, Pawtuckaway, Rollins Park, and Walmart sites, are illustrated in Fig. 9. Interspersed over the 10 min sampling period it appears that there are a number of relatively short intermittent periods of increased fluctuations, and, as discussed above, the causes of such behavior remain unknown. Then, the more rapid fluctuations exhibited at Hood Park in comparison with that at Rollins Park are presumably due to the stronger cross-winds along various multipath propagation paths. A number of unexplained anomalous features, which are shown in Fig. 10, were observed at the Beaver Brook, Hampton Beach,

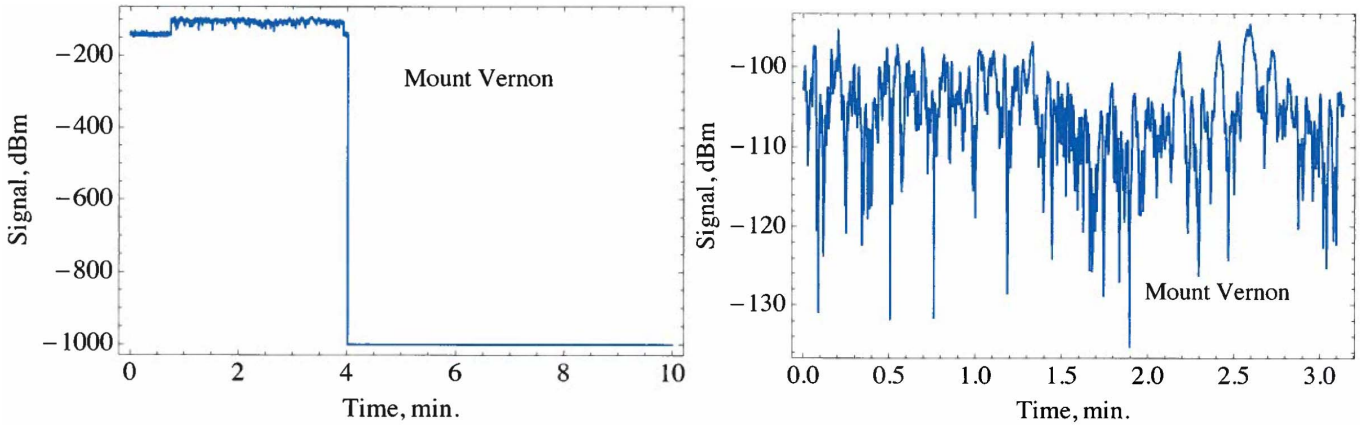

Fig. 11. Raw and filtered signal time series observed at the Mount Vernon, New Hampshire site. The abrupt received power reduction from about 4 to 10 min was due to a corresponding RF power failure at the transmitter.

TABLE I

OBSERVED SI OF THE NEW HAMPSHIRE IS PRESENTED TOGETHER WITH THE MEAN POWER LOSS AND MAXIMUM ENHANCEMENT ABOUT THE MEAN OBTAINED FROM THE CORRESPONDING (INDICATED) DATA RECORD LENGTH. IN SITES WHERE MORE THAN ONE 10 MIN OF SIGNAL DATA WAS RECORDED, ONLY THE CASE OF THE LARGEST OBSERVED SI IS LISTED

Date	Local Time	New Hampshire Location	Distance to AFSCN (km)	Data Record Length (min)	*SI*	Mean Power loss (dBm)	Max Enhancement (dB)
27-Apr	14:00-1500	Beaver Brook	26.7	8.61	0.80	-127.4	9.3
	17:00-18:00	Mount Vernon	6.54	3.14	1.28	-103.5	9.4
28-Apr	10:00-11:00	Rollin State Park	48.1	10	0.28	-99.9	4.4
	16:00-18:00	Walmart/Concord	43.2	10	0.0011	-84.9	0.42
29-Apr	9:00-10:30	Fort Stark State Beach	75.5	10	0.91	-116.3	9.3
	12:00-13:30	Hampton Sate Beach	66.8	9.72	0.80	-127.1	9.5
30-Apr	10:00-11:30	Pawtuckaway State Park	40.0	3.75	0.23	-118.1	3.5
	14:00-15:30	Youngsville Park-1	19.7	4.72	0.71	-128.6	9.3
	14:00-15:30	Youngsville Park-2	19.7	7.06	1.07	-127.2	9.7
	17:00-18:30	Hood Park	25.4	10	0.24	-127.8	7.2

and Youngsville sites. Examination of the signals from the Beaver Brook, Hampton Beach, and Youngsville sites reveals remaining rather abrupt increase/decrease in signal power that is out of character with the majority of the time series data. Different multipath signal variations indicated in Fig. 9 are all due to the multipath effects each of which depends on site-specific terrain, vegetation, and weather. It would be quite complicated to draw and generalized correlations between specific site conditions and RF fluctuations and is beyond the scope of this paper. The cause of these anomalies is unknown, and they are culled out in the ensuing data analysis given below in order to minimize the effects of unwanted nonstationary conditions. The times series data for the Mount Vernon site shown in Fig. 11 reveal three distinct segments. Analysis of the data contained in the first segment of 75 s reveals that it consists of uncorrelated white noise, while the third segment contains no data. The second segment, however, of about 3.14 min reveals valid data; this is presented in Fig. 11.

B. Multipath Scintillation

In Tables I and II, the SIs of both the New Hampshire and California sites are presented together with the mean power loss and maximum enhancement about the mean obtained from the corresponding (indicated) data record length. In sites where more than one 10 min sample of signal data was recorded (e.g., Mount Vernon and Rollin Park), only the case of the largest observed SI is listed in Table I. Examination of Tables I

TABLE II

SI OF CALIFORNIA SITES IS PRESENTED TOGETHER WITH THE MEAN POWER LOSS AND MAXIMUM ENHANCEMENT ABOUT THE MEAN OBTAINED FROM THE CORRESPONDING (INDICATED) DATA RECORD LENGTH. ONLY SITES WITH ENHANCEMENTS GREATER THAN 6 dB ARE LISTED. IN SITES WHERE MORE THAN ONE 10 MIN OF SIGNAL DATA WAS RECORDED, ONLY THE CASE OF THE LARGEST OBSERVED SI IS LISTED

Date	Local Time	California Location	Distance to AFSCN (km)	Data Record Length (min)	*SI*	Mean Power loss (dBm)	Max Enhancement (dB)
25-July	16:00	Santa Barbara Low Mast	75.3	10	1.01	-112.8	8.9
26-July	13:00	Santa Barbara	76.1	10	0.84	-109.4	8.6
28-July	18:00	Paso Robles	96.1	10	0.63	-110.3	8.7
25-July	13:00	Goleta Beach	76.1	10	0.24	-84.3	6.7

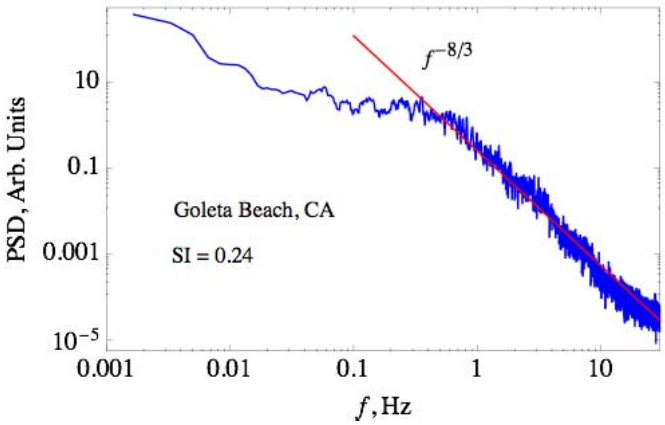

Fig. 12. Representative multipath PSD at various receiving sites.

and II reveals that the SI is highly site dependent and spans a range of 4 orders of magnitude from weak scintillation conditions (SI $\ll$ 1) to strong scintillation SI on the order or greater than unity. Note that sites where the SI that approaches and exceeds unity can occur at any time during the day. Weather conditions were clear for all of the measurements. In contrast to the clear line-of-sight scintillation, where the SI increases as $L^{11/6}$, the multipath SI bares no corresponding relationship. As previously alluded to, multipath scintillation is highly dependent on the temporally changing phase relationship between various multipath components. According to the Kolmogorov turbulence model, the relative strength of an index of refraction fluctuation of characteristic scale size "r" increases as $r^{2/3}$ for $\ell_0 < r < L_0$, where ℓ_0 and L_0 are the inner and outer scales of turbulence, respectively. In the lower atmospheric boundary layer, the inner and outer scales are of the order from a few millimeters to 1 cm, while the outer scale $L_0 \sim 0.4H$, where H is the height above ground [8]. For the sites under consideration here, H is typically about 50–100 m.

The multipath phase interference of these large eddies is primarily responsible for the resulting large values of the SI. This can be seen in the measured scintillation power spectra, where the PSD increases strongly at low frequencies, in contrast to the PSD of clear line-of-sight propagation paths illustrated in Fig. 2. Typical multipath power spectra are shown in Fig. 12 that illustrate the effects of multipath phase interference at low frequencies. The power spectra are the remnants of the Kolmogorov high-frequency falloff $\propto f^{-8/3}$ due to amplitude fluctuations along various indirect propagation paths. Because the integral of the PSD over all frequencies equals the SI, it is clear that the low-frequency contribution to the SI outmasks the corresponding contribution at higher frequencies.

C. Multipath Power Probability Distributions

Several probability distributions have been proposed in the literature that well describe the statistics of microwave signals under various multipath propagations conditions [9]. Among them are the Rayleigh, Rician, log-normal, Weibull, Nakagami-m [10], and the gamma–gamma distributions. In view of the body of the empirical evidence observed at various collection sites, the Rayleigh and Rician distributions can be eliminated *a priori*. The Rayleigh distribution refers to the electromagnetic amplitude, which implies that the corresponding power distribution obeys negative exponential statistics. However, the SI of the negative exponential distribution is unity, in contrast to various SI values displayed in Tables I and II. The Rician distribution can be eliminated by noting that it can be shown that this distribution does not admit an SI >1 [11], which is in contrast to measurements (e.g., Mount Vernon, Youngsville, and Santa Barbara sites). Also, as shown in the Appendix, the Weibull distribution does not fit the measured data and is, therefore, rejected as a viable candidate to describe multipath scintillation encountered in this measurement campaign. The Nakagami-m distribution is relatively new, being first proposed in 1960 [12]. It has been used to model the attenuation of microwave signals traversing multiple paths. The gamma–gamma distribution is a generalization of the gamma distribution for strong scintillation conditions [13].

The Nakagami-m distribution, which is a special case of the gamma distribution, was discovered by analyzing the fading of short-wave radio signals reflected in the ionosphere, and it is now known that it describes a wider class of electromagnetic signals that are modulated randomly by transmission or reflection due to multiple paths. This fading distribution has gained a lot of attention lately because the Nakagami-m distribution

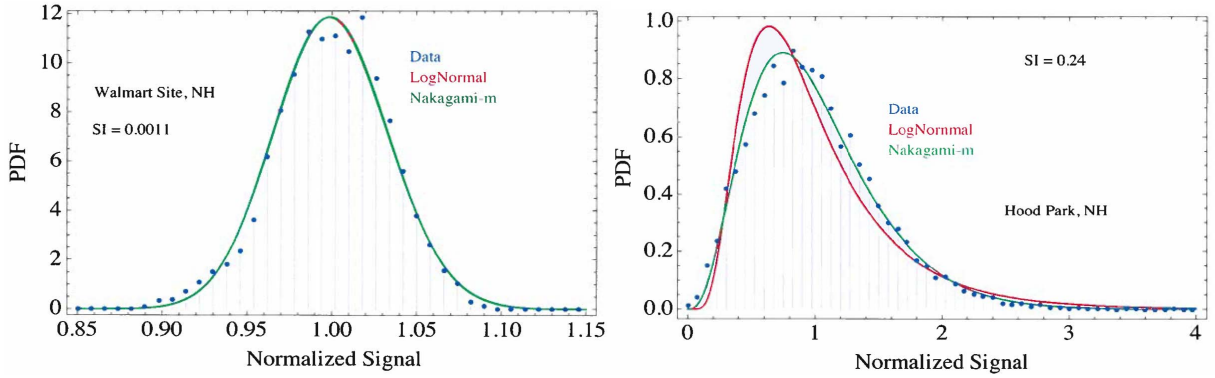

Fig. 13. Signal time series observed at the Mount Vernon, New Hampshire site.

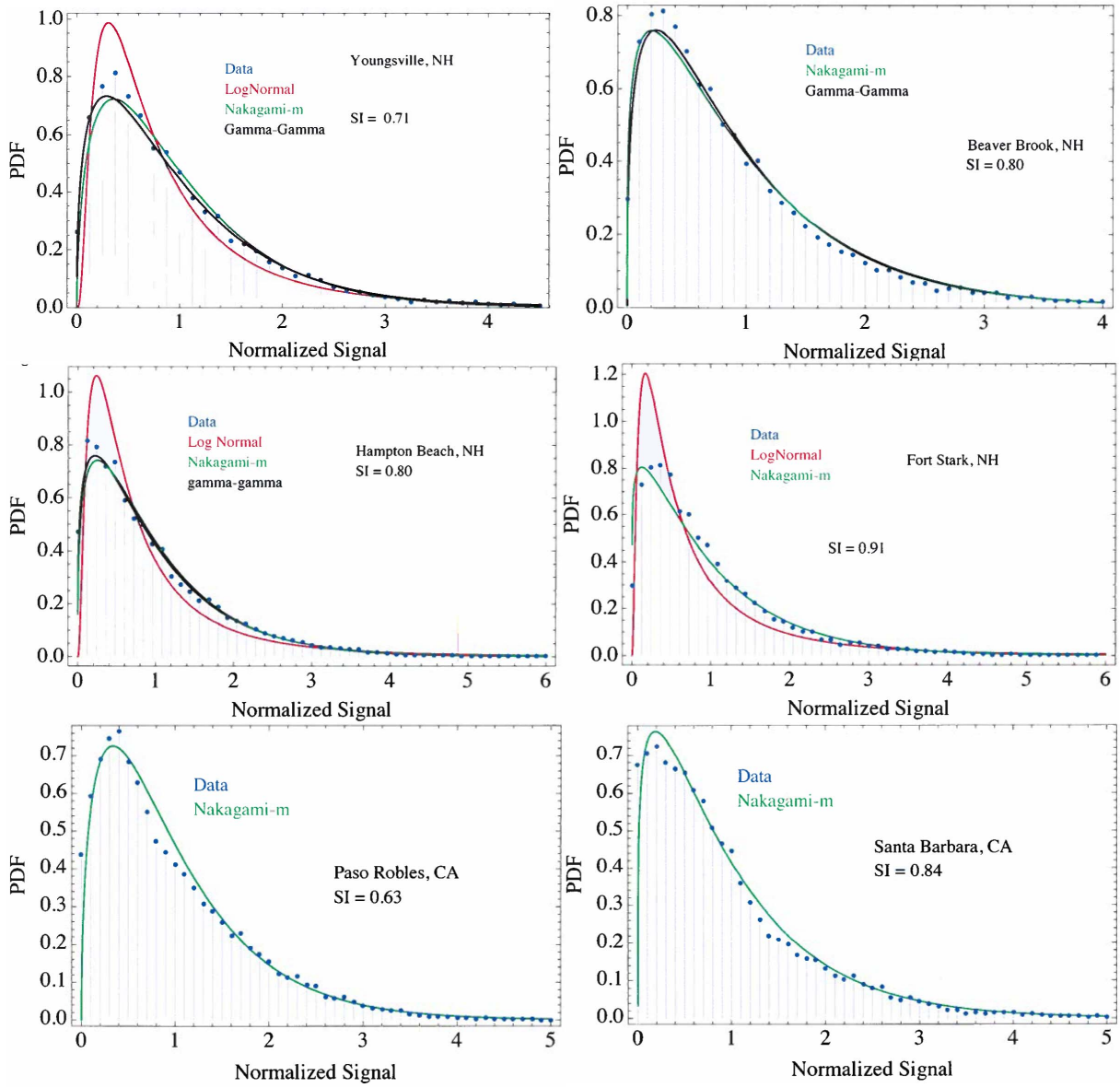

Fig. 14. PDF comparisons of weak–moderate scintillation conditions.

often gives the best fit to land-mobile and indoor-mobile multipath propagation as well as scintillating ionospheric radio links. It is important to note that the Nakagami-m is a purely phenomenological description. It was developed to fit experimental data; no one has yet succeeded in deriving it from the first principles as, for example, in the way, we were led to the log-normal distribution that was derived for tropospheric turbulence-induced clear line-of-sight optical

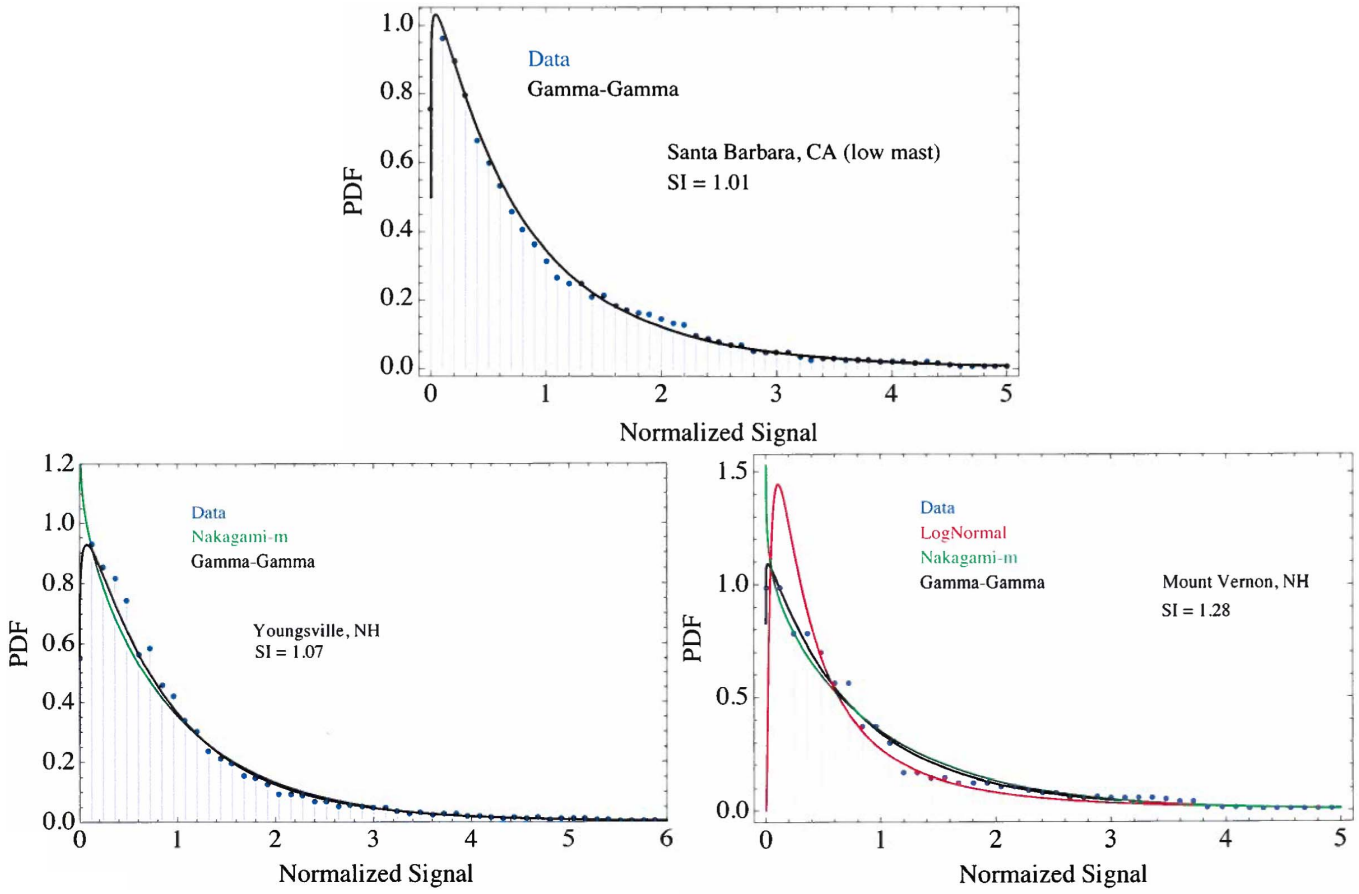

Fig. 15. PDF comparisons of strong scintillation conditions.

scintillation in the weak scattering regime. It is being given a special attention here for its ease of manipulation and wide range of applicability.

As we see, the observed power distributions are very well approximated by the Nakagami-m distribution under weak-to-moderate (SI < 0.6–0.9) multipath scintillation conditions. For moderate scintillations conditions (SI > 0.6–0.9), the observed SI is well approximated by both the Nakagami-m and the gamma–gamma distribution, which is a generalization of the gamma distribution strong scintillation conditions. For strong scintillation conditions (SI > 1), only the gamma–gamma distribution gives a valid description of the data. It has been shown in [2] that the log-normal distribution is applicable to clear line-of-sight propagation paths under weak scintillation conditions at several receiving sites, and for reference purposes is compared with the observed distributions. In the following, for technical simplicity, the received signal power at various sites is normalized to its mean.

In the following, x denotes the signal power normalized to its mean (i.e., $x = P/\langle P \rangle$). The corresponding probability density functions (PDF) of the Nakagami-m, the gamma–gamma, and the log-normal distributions are given in the following.

Nakagami-m Distribution:

$$p_N(x) = \frac{m^m x^{m-1}}{\Gamma(m)} \exp(-mx) \tag{5}$$

where $m = 1/\mathrm{SI}$ and $\Gamma(\cdot)$ denotes the gamma function.

Gamma–Gamma Distribution:

$$p_{GG}(x) = \frac{2(ab)^{(a+b)/2}}{\Gamma(a)\Gamma(b)} x^{(a+b)/2} K_{a-b}(2\sqrt{abx}) \tag{6}$$

where

$$\frac{1}{a} + \frac{1}{b} + \frac{1}{ab} = \mathrm{SI}. \tag{7}$$

$K_{a-b}(\cdot)$ is a modified Bessel function of the second kind.

Log-Normal Distribution:

$$p_{1n}(x) = \frac{1}{\sqrt{2\pi\sigma_{1n}^2}} \frac{1}{x} exp\left[-\frac{1}{\sigma_{1n}^2}\left(log\, x + \sigma_{1n}^2/2\right)^2\right] \tag{8}$$

where "log" denotes the natural logarithm and σ_{1n}^2 is given via (2) by

$$\sigma_{1n}^2 = log(1 + \mathrm{SI}). \tag{9}$$

The PDFs obtained from the measured data are compared with theoretical predictions given above and are shown for weak, moderate, and strong scintillation conditions in Figs. 13–15, respectively.

Examination of Fig. 13 reveals that the Nakagami-m distribution provides a reasonably good description for the weak scintillation data.[1] For weak-to-moderate scintillation conditions shown in Fig. 14, either the Nakagami-m or the gamma–gamma distribution provides a good fit to the data, while for

[1]Note for an SI $\ll$ 1 (e.g., the Walmart data), the Nakagami-m and the log-normal distributions are virtually identical.

TABLE III

COMPARISON OF THE NEW HAMPSHIRE SITES OF THE OBSERVED AND THEORETICALLY PREDICTED (IN PARENTHESIS) PERCENTAGE OF TIME THAT THE POWER EXCEEDS THE MEAN BY 3 AND 6 dB, RESPECTIVELY, TOGETHER WITH THE PROBABILITY DISTRIBUTION EMPLOYED FOR THE THEORETICAL COMPARISON

Date	Local Time	New Hampshire Location	SI	Probability Distribution	Percentage of Time Signal > 3dB, %	Percentage of Time Signal > 6dB
27-Apr	14:00-1500	Beaver Brook	0.80	Nakagami-m	11.4 (12.3)	1.2 (1.35)
	17:00-18:00	Mount Vernon	1.28	Gamma-Gamma	14.8 (13.9)	2.48 (2.24)
29-Apr	9:00-10:30	Fort Stark State Beach	0.91	Nakagami-m	12.86 (12.84)	1.60 (1.42)
	12:00-13:30	Hampton Sate Beach	0.80	Nakagami-m	12.5 (12.3)	1.0 (1.16)
30-Apr	14:00-15:30	Youngsville Park-1	0.71	Nakagami-m	11.3 (10.9)	1.04 (0.89)
	14:00-15:30	Youngsville Park -2	1.07	Gamma-Gamma	12.5 (13.2)	2.40 (2.24)

TABLE IV

COMPARISON OF THE CALIFORNIA SITES OF THE OBSERVED AND THEORETICALLY PREDICTED (IN PARENTHESIS) PERCENTAGE OF TIME THAT THE POWER EXCEEDS THE MEAN BY 3 AND 6 dB, RESPECTIVELY, TOGETHER WITH THE PROBABILITY DISTRIBUTION EMPLOYED FOR THE THEORETICAL COMPARISON

Date	Local Time	California Location	SI	Probability Distribution	Percentage of Time Signal > 3dB, %	Percentage of Time Signal > 6dB
25-July	16:00	Santa Barbara Low Mast	1.01	Gamma-Gamma	14.1 (13.5)	2.1 (2.6)
26-July	13:00	Santa Barbara	0.84	Nakagami-m	13.1 (12.6)	1.21 (1.29)
28-July	18:00	Paso Robles	0.73	Nakagami-m	11.6 (10.8)	0.40 (0.63)
25-July	13:00	Goleta Beach	024	Nakagami-m	2.6 (3.9)	0.04 (0.01)

strong turbulence conditions, where the SI exceeds unity, only the gamma–gamma distribution provides a good description of the data. Except for propagation cases where SI $\ll 1$, it is clear in the New Hampshire PDF curves that the log-normal distribution does not fit the data and, therefore, is not depicted in the corresponding California PDF curves.

D. Multipath Level Crossing Statistics

In contrast to microwave communication system performance where multipath fading effects are of prime importance, here we are primarily interested in signal power enhancements. In particular, it is vital to characterize the power fluctuation in terms of enhancement statistics, where quantities such as the positive level crossing rate (LCR) and the mean dwell time (MDT) of such crossing are determined. Here, we define the positive LCR as the rate at which the power crosses above a given threshold level and the MDT as the average time at which the power stays above a threshold level. As discussed Section I, the primary interest, here, is the identification of the site locations where there are significant fluctuations of signal power about the mean. To this end, only sites where the observed signal power shows fluctuations in the excess of 6 dB above the mean are considered.

In general, the fraction of time that the power exceeds a given x_0 is given by

$$F(x_0) = \int_{x_0}^{\infty} p(x)dx. \tag{10}$$

where $p(x)$ is the PDF of interest.

For the Nakagami-m and gamma–gamma distributions, these quantities are given by

$$F_N(x_0) = \frac{\Gamma(m, mx_0)}{\Gamma(m)} \tag{11}$$

where $\Gamma(m, mx_0)$ is the incomplete gamma function, and

$$F_{GG}(x) = 1 - \frac{\pi \csc[\pi(a-b)]}{\Gamma(a)\Gamma(b)}[Q_1(x) - Q_2(x)] \tag{12a}$$

where

$$Q_1(x) = \Gamma(b)(abx_0)^b \, {}_1\tilde{F}_2(b; b+1, b-a+1; abx_0) \tag{12b}$$

$$Q_2(x) = \Gamma(a)(abx_0)^a \, {}_1\tilde{F}_2(a; a+1, a-b+1; \mathrm{ab}x_0) \tag{12c}$$

and ${}_1\tilde{F}_2(\cdot)$ is a generalized hypergeometric function [14].

For both the New Hampshire and the California data, we present, in Tables III and IV, a comparison of the observed

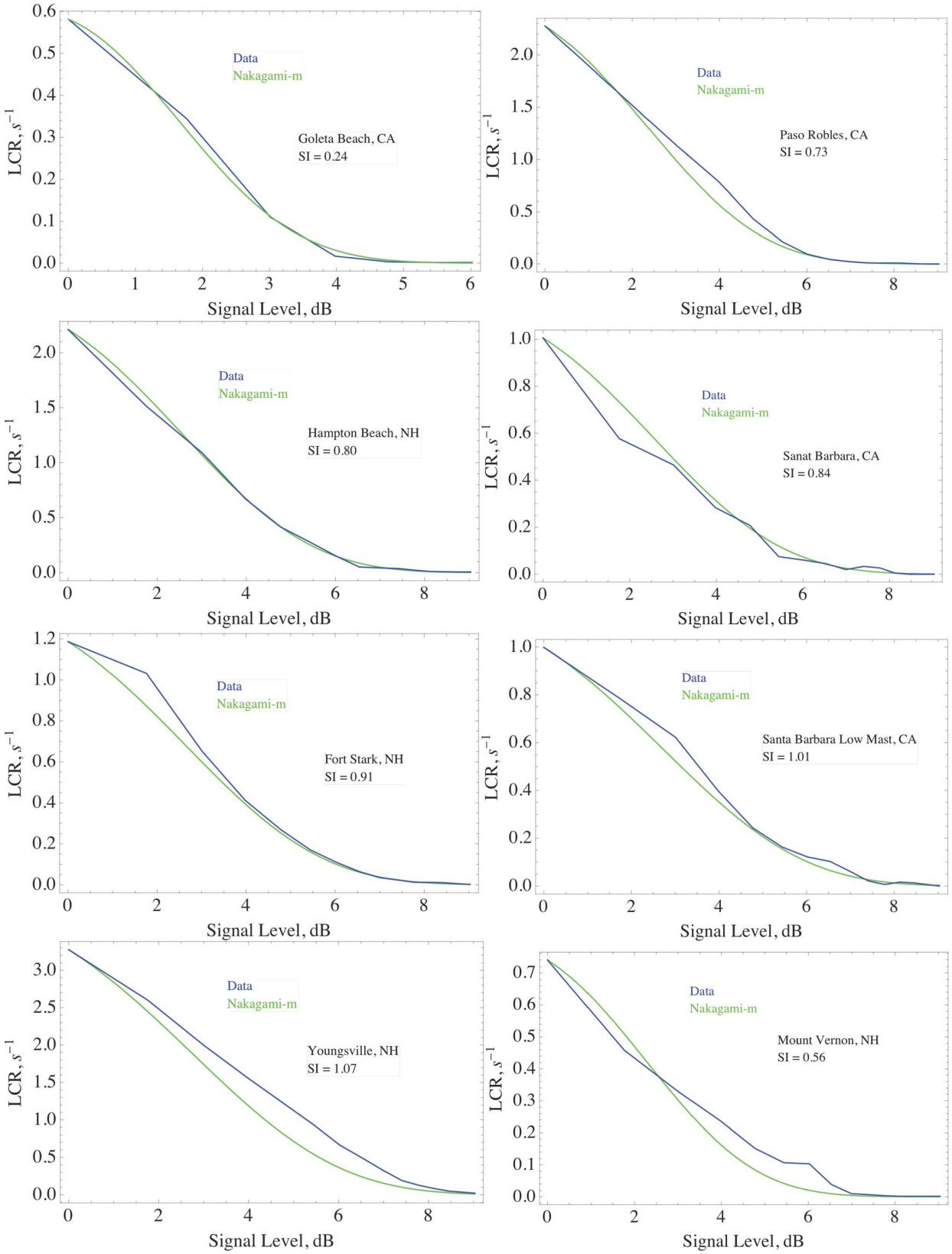

Fig. 16. Comparison of the measured and theoretically predicted LCRs for a wide range of SI values, both in California and New Hampshire.

and theoretically predicted (in parenthesis) percentage of time that the power exceeds the mean by 3 and 6 dB, respectively, together with the probability distribution employed for the theoretical comparison. Examination of Tables III and IV shows very good agreement with the measured data and theoretical predictions. As indicated in Tables III and IV,

TABLE V

COMPARISON OF THE NEW HAMPSHIRE SITES OF MEASURED AND PREDICTED LCR AND MDT VALUES FOR THE 3 dB LEVEL WHERE ENHANCEMENTS OF GREATER THAN 6 dB ABOVE THE MEAN WERE RECORDED

New Hampshire Location	SI	Observed LCR > 3 dB, s^{-1}	Theory: LCR > 3 dB, s^{-1}	Observed MDT, s	Theory: MDT, s
Youngsville Park-1	0.71	2.1	2.44	0.053	0.047
Hampton Sate Beach	0.80	1.09	1.07	0.11	0.11
Beaver Brook	0.80	2.25	2.52	0.20	0.22
Fort Stark State Beach	0.91	0.65	0.60	0.20	0.22
Youngsville Park -2	1.07	2.0	1.74	0.063	0.080
Mount Vernon	1.28	0.23	0.23	0.59	0.59

TABLE VI

COMPARISON OF THE CALIFORNIA SITES OF MEASURED AND PREDICTED LCR AND MDT VALUES FOR THE 3 dB LEVEL WHERE ENHANCEMENTS OF GREATER THAN 6 dB ABOVE THE MEAN WERE RECORDED

California Location	SI	Observed LCR > 3 dB, s^{-1}	Theory: LCR > 3 dB, s^{-1}	Observed MDT, s	Theory: MDT, s
Santa Barbara Low Mast	1.01	0.62	0.52	0.27	0.26
Santa Barbara	0.84	0.47	0.49	0.27	0.19
Paso Robles	0.73	1.14	0.99	0.10	0.11
Goleta Beach	0.24	0.11	0.11	0.20	0.35

TABLE VII

COMPARISON OF THE NEW HAMPSHIRE SITES OF MEASURED AND PREDICTED LCR AND MDT VALUES FOR THE 6 dB LEVEL WHERE ENHANCEMENTS OF GREATER THAN 6 dB ABOVE THE MEAN WERE RECORDED

New Hampshire Location	SI	Observed: LCR > 6 dB, s^{-1}	Theory: LCR > 6 dB, s^{-1}	Observed MDT, s	Theory: MDT, s
Youngsville Park-1	0.71	0.24	0.26	0.067	0.079
Hampton Sate Beach	0.80	0.15	0.15	0.067	0.074
Beaver Brook	0.80	0.34	0.35	0.039	0.033
Fort Stark State Beach	0.91	0.13	0.20	0.145	0.154
Youngsville Park -2	1.07	0.67	0.36	0.036	0.057
Mount Vernon	1.28	0.064	0.061	0.39	0.45

the power fraction above 3 and 6 dB of the mean is typically in the range of 10–14% and 1–2% of the time, respectively. We note that for all the other receiving sites, the measured SI is less than 0.2, which implies that the probability of obtaining a 6 dB or greater power enhancement is $< 1.7 \times 10^{-5}$, which is not of practical concern.

The positive (and negative) LCR for the Nakagami-m distribution is given by [15]

$$LCR_N(x_0) = \frac{\sqrt{2\pi}\, f_{eff}}{\Gamma(m)} (m x_0)^{m-1/2} \exp(-m x_0) \qquad (13)$$

where f_{eff} is an "effective channel Doppler frequency spread for the multipath propagation conditions of the link, and is given by $v_{eff} f_0/c$, where f_0 is the electromagnetic frequency (here 1.78 GHz), c is the speed of light in the atmosphere, and v_{eff} is the magnitude of an effective velocity parallel to the propagation direction. As indicated in (13), the LCR is directly proportional to the magnitude of an "effective" longitudinal velocity component that determines the Doppler frequency. We have no independent knowledge of this quantity, but, in general, it is not related to the longitudinal wind speed at the transmitter or the receiver; rather, it results from the longitudinal component of the motion of reflecting objects and corresponding wind components along various indirect paths. In order to effectively compare the measured level crossing statistics to the corresponding results based on the Nakagami-m distribution, we determine the effective LCR from the requirement that the measured and theoretical LCR are equal at the mean power level (i.e., 0 dB), and then use this value proceed to obtain the corresponding LCR at enhanced levels above the mean (i.e., 0 dB), and then compare these quantities at enhanced levels above the mean.

To the best of our knowledge, the corresponding LCR for gamma–gamma distribution does not appear in the literature.

TABLE VIII

COMPARISON OF THE CALIFORNIA SITES OF MEASURED AND PREDICTED LCR AND MDT VALUES FOR THE 6 dB LEVEL WHERE ENHANCEMENTS OF GREATER THAN 6 dB ABOVE THE MEAN WERE RECORDED

California Location	SI	Observed LCR > 6 dB, s^{-1}	Theory: LCR > 6 dB, s^{-1}	Observed MDT, s	Theory: MDT, s
Santa Barbara Low Mast	1.01	0.12	0.10	0.17	0.18
Santa Barbara	0.84	0.061	0.072	0.24	0.18
Paso Robles	0.73	0.093	0.089	0.041	0.072
Goleta Beach	0.24	0.0017	0.0031	0.25	0.20

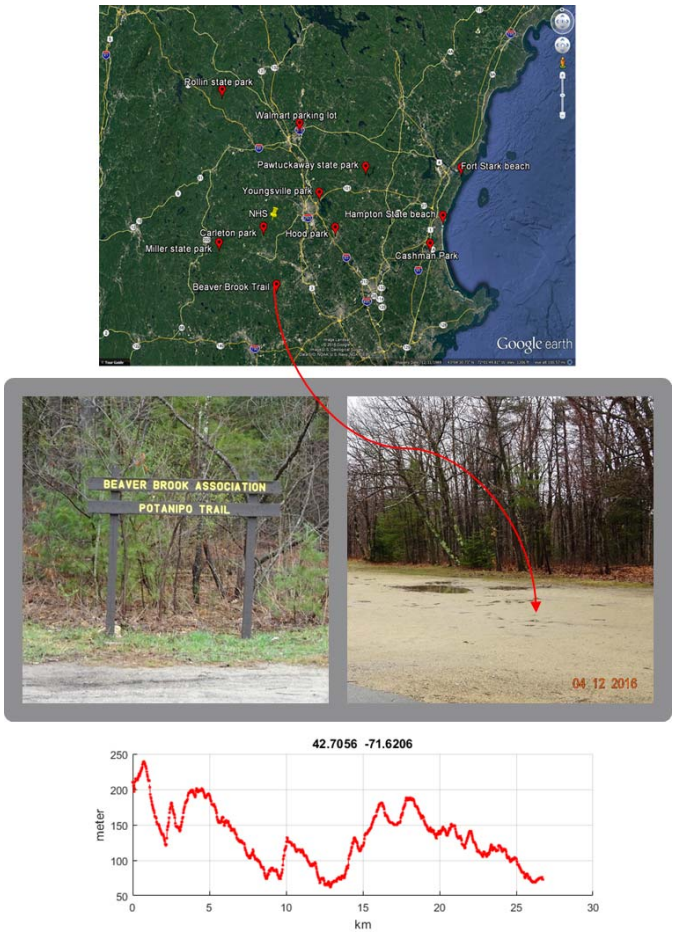

Fig. 17. Map and terrain profile for the path between the transmitter, NHS, and the receiver at Beaver Brook, New Hampshire. The terrain map clearly shows the lack of direct line of sight between the transmitter at the left of the profile (0 km) and the receiver at the right terminus of the profile (~26 km). The photographs show the surroundings at the receiver site which consisted of dense woods.

Surprisingly, however, as is indicated in the following, the LCR of the Nakagami-m distribution, even for cases where SI > 1, is in very good agreement with measured LCRs and is used here as an engineering approximation for the gamma–gamma LCR.

In addition, the MDT is obtained directly from the fraction of time that the power exceeds x_0, F(x_0), and the corresponding LCR, and is given by

$$MDT(x_0) = \frac{F(x_0)}{LCR(x_0)} \tag{14}$$

The measured and theoretically predicted LCRs are compared in Fig. 16 for a wide range of SI values, in both California and New Hampshire. Examination of Fig. 16 reveals that the Nakagami-m LCR is in very good agreement with measurements for weak-to-moderate-to-strong multipath scintillation conditions. For receiving locations where enhancements of greater than 6 dB above the mean were recorded, comparisons of measured and predicted LCRs and MDTs are presented in Tables V and VI for the 3 dB level and in Tables VII and VIII for the 6 dB level. For all cases of interest, the Nakagami-m LCR is well within a factor of 2 of the measured values.

IV. DISCUSSION AND CONCLUSION

For all but one of the 19 sites in both California and New Hampshire, there is no direct clear line-of-sight links between the RF source transmitter and the receiver, and thus the corresponding signal results from various indirect multipaths. A representative map and terrain profile for a no clear line-of-sight link is shown in Fig. 17. The observed SI at various surrounding receiving sites shows a wide range of values that are orders of magnitude larger than what one would expect for clear line-of-sight propagation paths. Furthermore, the probability distributions of the corresponding power fluctuations are well approximated by the Nakagami-m and the gamma–gamma distributions for weak-to-moderate and weak-to-strong scintillation conditions, respectively. In particular, the measured data at all of the receiving sites do not support the use of the negative exponential power (Rayleigh in signal amplitude) distribution. In the literature, Rayleigh fading is viewed as a reasonable model for tropospheric signal propagation on radio signals and is most applicable when there is no dominant propagation along a line of sight between the transmitter and receiver [16], [17]. This result, however, is based on a central limit theorem argument for the received multipath signal and is valid in practice if both the number of independent terms n comprising the signal $\sum_{j=1}^{n} A_j e^{i\phi_j}$ is large and $\langle A_j^2 \rangle \ll \sum_{j=1}^{n} \langle A_j^2 \rangle$ for all j; i.e., in the sum, there are no predominant term(s) [18]. Apparently, the multipath signals observed in both the rural/suburban environments of California and New Hampshire do not satisfy either of these two conditions or both. As indicated in Section III-A, various short-term signal anomalies/artifacts were occasionally observed. At present, these are unaccounted for and were not included in the subsequent data signal analyses.

We have identified those sites where enhancement levels of greater than 6 dB above the mean power level were observed at any time during the day. This identification is important in the context of this paper, because propagation models, which only provide a mean value of power, do not predict enhanced RF power. Therefore, they must be taken into account when looking at potential interference between transmitters and receivers. In contrast to clear line-of-sight propagation, cases where the observed multipath SI approaches and exceeds unity can occur anytime during the day. In addition, as opposed to measurements taken over long time periods [19], because of the relatively short-term measurement periods, the results obtained to date do not necessarily represent the long-term situation. In particular, whether or not >6 dB power enhancements at other sites can be expected is not addressed by the current analysis. Nor is the ability of the analysis to predict *a priori* the likelihood of such enhancements addressed. The observed probability distributions of multipath scintillation are compared with several candidate distributions, and the Nakagami-m and the gamma–gamma distribution emerge as the preferred distributions for weak-to-moderate and moderate-to-strong scintillation conditions, respectively. The observed level crossing statistics of the multipath signal is compared with theory, where good agreement (well within a factor of 2) is obtained for the fraction of time the signal remains above a given threshold, and both the corresponding LCR and MDT.

Finally, in contrast to the RF regime, where the observed line-of-sight fluctuations are driven by humidity fluctuations, in the optical regime, temperature fluctuations are primarily responsible for phase and amplitude fluctuations, which are not uniquely correlated with humidity fluctuations. As such, line-of-sight monochromatic optical scintillation predictions based on RF measurements are, at best, tenuous. In addition, corresponding optical signals are much narrower and do not significantly penetrate terrain resulting in which virtually no multipath effects would be obtained over the nonline-of-sight propagation paths encountered in this paper.

Appendix
Weibull Distribution

The Weibull distribution used in wireless communications has been purported to show in empirical studies to be an effective model in both outdoor [20] and indoor [21] environments. The PDF of the Weibull distribution for the signal normalized to its mean is given by

$$p_w(x) = \frac{\alpha}{\beta}(x/\beta)^{(\alpha-1)}\exp[-(x/b)^{\alpha}] \tag{A.1}$$

where

$$\beta = 1/\Gamma(1+1/\alpha) \tag{A.2}$$

and

$$\frac{\Gamma(1+2/\alpha)}{\Gamma(1+1/\alpha)} - 1 = \mathrm{SI}. \tag{A.3}$$

Note that for $\alpha = 1$, the Weibull distribution becomes the negative exponential distribution.

To show that the Weibull distribution is not a valid distribution to describe the multipath scintillation encountered in this measurement campaign, we compare the PDF of the data, corresponding to weak-to-moderate, weak-to-moderate, and weak-to-strong scintillation conditions to the Weibull distribution, consistent with (A.2) and (A.3), the Nakagami-m and the gamma–gamma distributions. Figs. 18–20 show this comparison for the weak-to-moderate, weak-to-moderate and weak-to-strong scintillation conditions, respectively. Examination of Figs. 18–20 clearly reveals that the Weibull distribution does not adequately describe the data for a wide range of

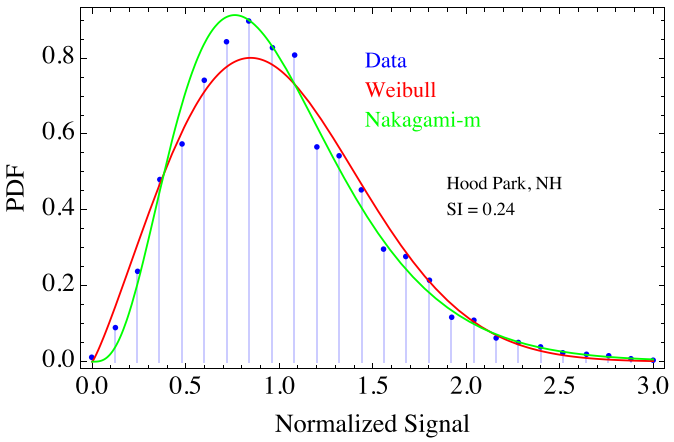

Fig. 18. Comparison of the PDF of the Weibull and gamma distributions to the measured data for weak–moderate scintillation conditions.

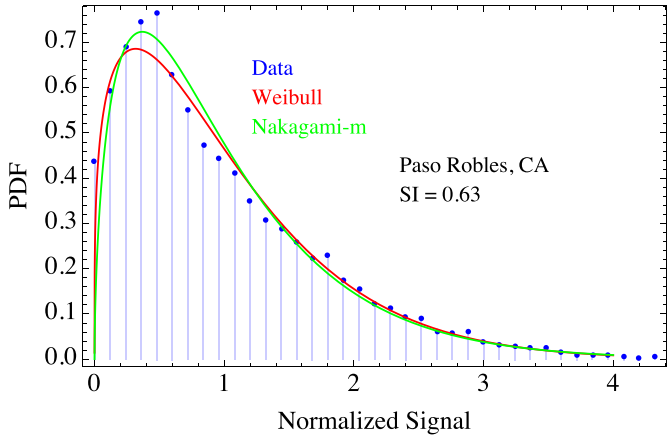

Fig. 19. Comparison of the PDF of the Weibull and gamma distributions to the measured data for moderate scintillation conditions.

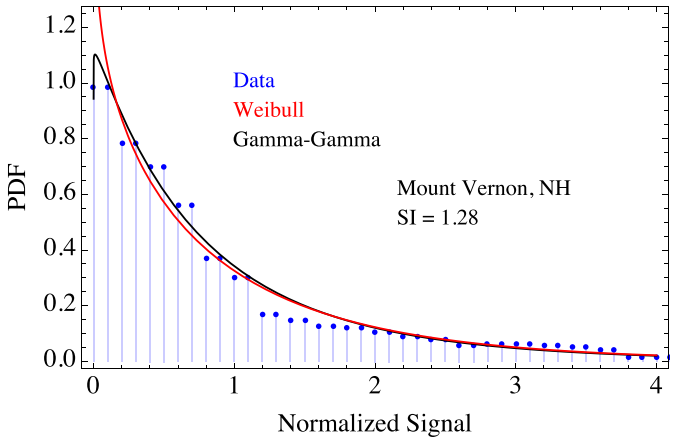

Fig. 20. Comparison of the PDF of the Weibull and gamma distributions to the measured data for strong scintillation conditions.

scintillations conditions. Therefore, we reject the Weibull distribution as a suitable candidate for describing multipath scintillation statistics.

ACKNOWLEDGMENT

The authors would like to thank Dr. V. Lang for her organization and inception of this paper.

REFERENCES

[1] *Propagation Data and Prediction Methods Required for the Design of Terrestrial Line-of-Sight Systems*, document Rec. ITU-R P.530-16 (07/2015).
[2] V. I. Tatarski, *Wave Propagation in a Turbulent Medium*. New York, NY, USA: Dover, 1961, pp. 40–55.
[3] A. D. Wheelon, *Electromagnetic Scintillation; I. Geometrical Optics*. Cambridge, U.K.: Cambridge Univ. Press, 2001, ch. 2, pp. 55–57.
[4] A. D. Wheelon, *Electromagnetic Scintillation; II. Weak Scattering*. Cambridge, U.K.: Cambridge Univ. Press, 2003, ch. 3, pp. 311–312.
[5] A. D. Wheelon, *Electromagnetic Scintillation; II. Weak Scattering*. Cambridge, U.K.: Cambridge Univ. Press, 2003, ch. 3, pp. 311–312.
[6] M. C. Thompsen, F. E. Marler, and K. C. Allen, "Measurements of the microwave structure constant profile," *IEEE Trans. Antennas Propag.*, vol. AP-28, no. 2, pp, pp. 278–280 Mar. 1980.
[7] J. A. Lane, A. C. Gordon-Smith, and A. M. Zavody, "Absorption and scintillation effects at 3 mm wavelength on a short line-of-sight radio link," *Electron. Lett.*, vol. 3, no. 5, pp. 185–186, May 1967.
[8] A. D. Wheelon, *Electromagnetic Scintillation; I. Geometrical Optics*. Cambridge, U.K.: Cambridge Univ. Press, 2001, ch. 2, pp. 78–80.
[9] *Multipath Propagation*. Accessed: Oct. 11, 2018. [Online]. Available: https://en.wikipedia.org/wiki/Multipath_propagation
[10] A. D. Wheelon, *Electromagnetic Scintillation; II. Weak Scattering*. Cambridge, U.K.: Cambridge Univ. Press, 2003, ch. 3, pp. 349–352.
[11] A. D. Wheelon, *Electromagnetic Scintillation; II. Weak Scattering*. Cambridge, U.K.: Cambridge Univ. Press, 2003, ch. 3, pp. 346–347.
[12] M. Nakagami, "The M-distribution—A general formula of intensity distribution of rapid fading," in *Statistical Methods of Radio Wave Propagation*, W. C. Hoffman, Ed. Oxford, U.K.: Pergamon Press, 1960.
[13] L. C. Andrews, R. L. Phillips, and C. Y. Hopen, *Laser Beam Scintillation With Applications*, Bellingham, WA, USA: SPIE, 2001, pp. 88–92.
[14] S. Wolfram, *Wolfram Mathematica, Version 9*. Cambridge, U.K.: Cambridge Univ. Press, 2012.
[15] M. D. Yacoub, C. R. C. M. da Silva, and J. E. V. Bautista, "Second-order statistics for diversity-combining techniques in Nakagami-fading channels," *IEEE Trans. Veh. Technol.*, vol. 50, no. 6, pp. 1464–1470, Nov. 2001.
[16] J. G. Proakis, *Digital Communications*, 3rd ed. Singapore: McGraw-Hill, 1995, pp. 767–768,
[17] B. Sklar, "Rayleigh fading channels in mobile digital communication systems I. Characterization," *IEEE Commun. Mag.*, vol. 35, no. 7, pp. 90–100, Jul. 1997.
[18] P. Beckmann, *Probability in Communication*. San Diego, CA, USA: Hartcourt, 1967, pp. 106–107.
[19] K. L. Ho, N. D. Mavrokoukoulakis, and R. S. Cole, "Propagation studies on a line-of-sight microwave link at 36 GHz and 110 GHz," *IEE J. Microw., Opt. Acoust.*, vol. 3, no. 3, pp. 93–98, May 1979.
[20] N. S. Adawi *et al.*, "Coverage prediction for mobile radio systems operating in the 800/900 MHz frequency range," *IEEE Trans. Veh. Technol.*, vol. 37, no. 1, pp. 3–72, Feb. 1988.
[21] H. Hashemi, "The indoor radio propagation channel," *Proc. IEEE*, vol. 81, no. 7, pp. 943–968, Jul. 1993.

Authors' photographs and biographies not available at the time of publication.